

First results with 'imaka

M. Chun^a, J. R. Lu^b, M. Service^a, O. Lai^c, D. Toomey^d, F. Abdurrahman^b, C. Baranec^b, and
D. Fohring^b

^aInstitute for Astronomy, University of Hawaii, Manoa

^bUniversity of California, Berkeley

^cObservatoire de la Cote d'Azur, Nice, France

^dMauna Kea Infrared LLC, Hilo, HI 96720

ABSTRACT

We present first-light results from 'imaka, the wide-field ground-layer adaptive optics (GLAO) demonstrator on the University of Hawaii 2.2-meter telescope on Maunakea, Hawaii. Natural guide star asterisms with diameters of 10-16 arcminutes were tested. Focal plane images sampling the central $\sim 10'$ show image resolution improvements of a factor of 1.3-2.7 under a variety of seeing conditions and for wavelengths from 0.6 to 1 micron. Analysis of telemetry data from the system confirms that the ground layer is thin (<100 m) and that the dominant residual errors are the residual free-atmosphere and the tomographic reconstruction error.

Keywords: adaptive optics

1. INTRODUCTION

Adaptive optics systems are now moving toward larger corrected fields of view. Ground-layer adaptive optics (GLAO) is an emerging approach that trades the amount of residual wavefront error for the size of the corrected field of view by selectively correcting for turbulence that arises close to the telescope. In recent years, several GLAO systems have been commissioned on-sky, including on the SOAR telescope with a $3' \times 3'$ field,¹ the Large Binocular Telescope (LBT) with a $4' \times 4'$ field,² and the Very Large Telescope (VLT) with a $7' \times 7'$ field.³ All have started, or will start, science operations soon.

Maunakea, Hawaii appears ideal for GLAO given the thinness of the ground layer and the weak optical turbulence in the free atmosphere.^{4,5} GLAO on Maunakea has the potential to reach fields of view of tens of arcminutes in diameter with spatial resolutions of the free-atmosphere seeing. This could be significantly larger than any other GLAO implementation. We present first-light results from the 'imaka project, which delivers GLAO correction over fields in excess of 15 arcminutes in diameter on Maunakea, Hawaii.

1.1 'imaka

'imaka is a test-bed wide-field adaptive optics system deployed at the Cassegrain focus of the University of Hawaii 2.2-meter telescope on Maunakea, Hawaii. The adaptive optics system consists of an optical relay with a $24' \times 18'$ oval guide star acquisition field of view, a 36-element curvature deformable mirror (DM) conjugate to the ground, and a set of five 8×8 subaperture Shack-Hartmann wavefront sensors deployed on natural guide stars distributed around the periphery of the field. The optical design, a "broken" Offner relay with unequal input ($f/10$) and output ($f/13.3$) f -numbers, has its image quality optimized over the center $11' \times 11'$ field but allows for wavefront sensing, with some fixed aberrations, in the periphery of the field. 'imaka can accommodate a variety of science cameras including a large CCD camera ($11' \times 11'$) and a Teledyne H4RG15-based camera ($7' \times 7'$) being prepared for the UH 2.2-meter telescope. These cameras are currently not commissioned so all of our 'imaka runs to date have used a smaller commercial CCD camera (Finger Lakes Instrumentation ML50100) that covers a $4' \times 5'$ field of view centered slightly off of the field center. The entire opto-mechanical system is housed in a custom carbon-fiber box that bolts to the bottom of the UH 2.2 m telescope. A more detailed description of the instrument's specifications can be found in.⁵

mchun@if.a.hawaii.edu

Lab integration of 'imaka took place during the Summer and Fall of 2016. Of note from the integration was the optical alignment of the mirrors within the 'imaka carbon-fiber (CF) structure. The structure consists of a set of flat CF panels with aluminum inserts or captured nut plates as interfaces for the mirror assemblies. The interfaces and the panels are positioned and glued during the structure assembly on a machined steel table with aluminum positioning fixtures. The end position accuracies of the mirror interface surfaces (0.25 mm) were poor compared to normal machine tolerances. As a result, the first step in the optical alignment included measuring and positioning each mirror using a portable coordinate measuring arm. All the elements up to the final sphere were aligned this way using the instrument's telescope interface plate as our mechanical reference. We aligned the final sphere and fold flat by optimizing the image quality and centering the optical beam on the output port. The resulting optical aberrations and the measured image quality across the field at the science camera were similar to that predicted from the optical design. An important element in this process was that the Offner relay has fairly loose alignment tolerances (0.1mm in separations and de-centers) and consists only of flat and spherical surfaces. For future GLAO instruments with tighter tolerances or off-axis elements, the 'imaka approach to the structure fabrication likely would not work and better metrology and/or machining of the optical interfaces would be needed. For example, machining of the aluminum interfaces after structure assembly is an option. These other approaches, however, were not within the budget scope of the 'imaka project.

In order to reduce the cost of the instrument, we made simplifications to the instrument that significantly impact the way we observe and use the system. In particular, the use of natural guide stars and fixed wavefront sensors (WFS) allowed us to avoid the expense and complexity of laser guide stars and mechanisms to position the WFSs. However these limit us to fields that contain sufficiently bright stars within the acquisition field of the instrument and effect how quickly we can reconfigure the system for a new field. Thus, 'imaka is limited to a handful of asterisms about the night sky and, in practice, to a single constellation per night.

The instrument's software architecture includes a command and data server which allows the instrument to be sequenced for calibrations, provides a means to read or write system parameters, settings, and allows recording of AO telemetry data that is synchronized with the science camera data stream. Up to eight different control matrices can be loaded at once and the system can be switched to any of these in a single step of the system. This makes it simple to compare different control schemes or different configurations of the guide stars with the system. An observation sequencer controls these settings (e.g. control matrix, gains, etc.) and sequences the recording of science camera and AO telemetry data. A typical data sequence will collect both science images (30-60 seconds long) and AO telemetry data (typically 15 seconds) while cycling through turning on/off the GLAO correction with a variety of AO settings (e.g. control matrix, gain, etc.). By cycling through this sequence of GLAO off/on data, we mitigate some of the variations in the seeing.

2. EXPECTED PERFORMANCE

We model the 'imaka performance using a combination of Monte-Carlo simulations⁶ and a detailed image quality error budget. The error budget contains the common AO error terms such as the bandwidth, fitting, and measurement errors but we note that the image quality is dominated by two GLAO specific residual phase errors - the residual uncorrected free-atmosphere seeing and the free-atmosphere seeing injected into the GLAO correction due to limits in the tomographic reconstruction. This latter term is especially important for natural guide star GLAO systems.⁷ In this section we briefly outline the dominant image quality error terms for 'imaka and note where specific design choices for the instrument have a significant impact. In particular we discuss separately the errors that are specific to our particular implementation and those that are specific to the GLAO correction.

As a precursor to this discussion we note that errors in our error budget are expressed as either RMS wavefront error (WFE) or as image full-width at half-maximum (FWHM). The residual WFE for a GLAO system is large compared to a classical adaptive optics system; the largest single error term, the residual free-atmosphere seeing, is typically 300-400 nm RMS or more. Thus the image FWHM is a more natural figure of merit. Since many of the common AO error terms are expressed in WFE, we carry both in our error budget. In the end we combine WFE and image FWHM to get the final estimate of the FWHM. The WFE does not uniquely convert to a FWHM. Here we do the conversion by assuming that the residual phase variance is described by $(D/r_{0,eff})^{5/3}$ and in turn that the $FWHM = 0.98\lambda/r_{0,eff}$. This assumption is likely only valid for the two largest terms in the

error budget – the residual free-atmosphere WFE and the free-atmosphere tomographic error which should have Kolmogorov like power spectra. For other terms such as the residual ground-layer phase variance, we expect that the higher-spatial order aberrations have a larger relative weight than from a Kolmogorov spectrum and we therefore underestimate the FWHM. In this paper, we ignore these effects and simply note that the total WFE from all terms other than the two largest errors is less than the WFE from the tomographic error. An abbreviated error budget is presented in (Table 1). For brevity we include only the significant or notable terms.

Many of these errors are implementation specific but all are relevant to any GLAO system. The notable “common” AO error terms for ‘imaka are the optical design field aberrations, the optical figure errors on the mirrors, pupil distortion errors, and the system bandwidth error. The first three rise in importance relative to a narrow-field AO system as a result of the large field of view passed by the system. They are challenges for any GLAO system implemented through an optical relay and they are also challenges for any wide-field instrument following the GLAO system. For example, all of the optics in the ‘imaka optical relay conjugate well away from the ground so their static figure errors are largely non-common path and are not corrected by the GLAO system. The large field of view of the instrument also makes it difficult to form a good pupil image over the full field. Pupil distortions amount to a shifting or misapplication of the DM correction for a given field footprint. Within the science field of view, the pupil distortions were designed to be $\lesssim \pm 1.5\%$. The field dependent phase error introduced by these distortions were estimated via simulations by shifting the DM correction with respect to the “correct” location and quantifying the resulting RMS phase error. The final large “common” AO error term that is specific to our implementation is the bandwidth error. For ‘imaka we implemented the wavefront sensors using in-hand commercial-grade Raptor Photonics Kite EMCCD cameras whose readout rate is limited by an overhead in the camera readout (4.3 msec for the 96×96 pixel subarray of the detector). The sampling rate of the system was usually between 150-180 Hz and the measured 0 dB bandwidth of the system, measured by closing the loop on noise in the WFS cameras, is $f_{0dB} \sim 15$ Hz. We estimate that the characteristic temporal frequency of the dome and ground layer are relatively long ($\tau_{GL} \sim 10 - 12$ msec)⁸ but the bandwidth of the system nonetheless remains one of the larger terms in the budget. We estimate that in total the implementation specific phase errors described here sum to 140nm RMS error. In image space, using the conversion described above, this error corresponds to an the image $FWHM_{imp} \sim 0.09''$.

An addition instrumental error comes from the lack of an atmospheric dispersion corrector in ‘imaka. We observe our fields over a full range of zenith angles ($ZA \leq 60$ degrees), and all of the images are in the visible. Across the two primary filters we observed with (R and I) the dispersion amounts to $0.2''$ and $0.12''$ at zenith angles of 45 degrees and $0.07''$ and $0.04''$ at zenith angles of 20 degrees. In the summary error budget (Table 1) these are not included (e.g. Zenith values).

As a final note on our implement, we acknowledge but have not quantified the error caused by the mismatch between the curvature DM actuator response functions and the Shack-Hartmann wavefront sensor. More than half of the DM actuators are outside the edge of the pupil so their signal in the Shack-Hartmann WFS is small. This mismatch manifests itself as a poorly conditioned inversion of the DM-WFS interaction matrix and limits our control to approximately 29 degrees of freedom (as opposed to the 36 actuators on the DM).

The large residual errors for GLAO are the uncorrected free-atmosphere, the residual ground-layer, and the tomographic error in the sensing of the ground-layer. For uncorrected free-atmosphere phase error we take the median free-atmosphere seeing of $0.33''$ at 0.5 microns measured by the MASS unit in the Maunakea seeing monitor. This value is derived from the first three years of operation of the MASS unit on the summit of Maunakea and it closely matches that found at the Maunakea 13N site during the Thirty-Meter Telescope (TMT) site characterization campaign.⁹ That seeing value corresponds to a phase variance of 410 nm RMS. For the residual ground-layer phase variance, there are two contributions - the fitting error and the isoplanatic error (the portion of the ground-layer that is conjugated too far from the DM to be corrected over the field of view). For the fitting error, we assume that the spatial power spectrum is Kolmogorov and use a standard estimate based on the the actuator pitch and an estimate of the ground-layer $r_{0,GL}$. The latter is derived from the integrated and free-atmosphere seeing at the time of the observation by the Maunakea seeing monitor. The assumption that the ground-layer turbulence is Kolmogorov is probably not true as dome and tube seeing is likely to not fully developed and may have a small wavefront outerscale. However, we have no direct measure of a deviation from Kolmogorov. For the portion of the ground-layer uncorrected by the GLAO system due to

Table 1. Error Budget Summary at $\lambda = 0.5\mu\text{m}$ at Zenith

Error Term	Estimated WFE (nm)	Estimated FWHM (as)	Phase Variance Model	Comment
Optical Design		0.09		Raytrace with common Zernikes removed at DM.
Implementation errors	140	0.09		Optics, pupil distortions, and bandwidth errors
Tomographic Error in FA	205	0.15	σ_{FA}^2/N_{WFS}	GLAO correction injects some FA into GLAO correction. $r_{0,FA} = 0.31$ m (0.33" FA seeing) and $N_{WFS}=4$.
Uncorrected FA (σ_{FA}^2)	410	0.33	$(\frac{D}{r_{0,FA}})^{5/3}$	Assume we can derive from MASS measurements.
Total	488	0.41	$(\frac{D}{r_{0,eff}})^{5/3}$	$\text{FWHM} = [\sum f_i^{5/3}]^{3/5}$

it being too far from the ground we assume that the ground layer is distributed so that 10% of this turbulence (namely induced phase variance) is above the first 30 meters¹⁰ and that it is entirely uncorrected by the GLAO system.

The second largest term in the GLAO error budget is the error we make in estimating the correction to apply due to the limited number of guide stars. For the data discussed in this paper the ‘imaka guide star asterisms lie on circles with diameters greater than 15 arcminute. For a 2.2-meter telescope, the meta pupils of these guide stars shear by a full pupil at an altitude of 1 kilometer. Given this and that the optical turbulence profile shows little turbulence between 100m and 1km¹⁰ we estimate the tomographic error to be simply the free-atmosphere phase variance divided by the number of guide stars. Namely, we treat the free-atmosphere contribution in the wavefront sensor measurements as uncorrelated noise whose variance averages down with the number of guide stars. Since we typically use between 3-5 guide stars, this error term is only a factor of two less than the free-atmosphere RMS error. This effectively increases in the free-atmosphere seeing.

The major error terms are summarized in table 1. In all but the optical design, we express the error in terms of a wavefront error and then derive an image blur via an effective r_0 as described earlier.

3. ON-SKY RESULTS

3.1 Observations

‘imaka was delivered to the UH 2.2 m telescope and installed in October 2016. Commissioning took place during two runs on 2016 Oct 20-24 UT (RUN1) and 2016 Nov 15-19 (RUN2) and GLAO observations were obtained during three observing runs on 2017 Jan 9-13 UT (RUN3), 2017 Feb 13-17 UT (RUN4), and 2017 May 17-22 UT (RUN5). During each of these runs we observed a single field over the course of each night. During RUN3 and RUN4, we targeted a field in the Pleiades cluster centered on $\alpha = 03\text{h } 48\text{m } 58.0\text{s}$, $\delta = +24^\circ 16' 00''$ (J2000) with an asterism of five bright stars distributed about the outside of the field of view on a circle of diameter of about 16-17 arcminutes. During RUN5, we targeted a denser star field towards the Galactic plane at $\alpha = 19\text{h } 33\text{m } 44.8\text{s}$, $\delta = +07^\circ 49' 46''$ (J2000), with four guide stars. In this case, the field was centered on one of these bright stars and it was either used as one of the GLAO guide stars or as a scoring/truth wavefront sensor. The three guide stars outside the science field of view roughly scribe a circle with diameter 15 arcminutes. Prior to each run, the wavefront sensors and the calibration unit were setup for the specific constellation of guide stars. Calibrations (e.g. centroid offsets and interaction matrices) and a new set of control matrices for different combinations of WFSs were made during the day before the beginning of each night.

Observations were made in sequences of different system configurations. The simplest change in configuration is turning on and off the GLAO correction (e.g. correction on and correction off) but a more complex sequence may include cycling through different control matrices or different asterisms of guide stars. Since the seeing varies with time, we repeat the sequence multiple times and averaged the results over the course of the night. A typical data set for one of these sequences is an GLAO-on and GLAO-off set of focal plane images (30-60

seconds) and AO telemetry data (e.g. WFS pixels, centroids, voltage errors, and accumulated DM voltages) covering the first 10-15 seconds of the focal plane image. Note that the GLAO-off data are always taken with the GLAO system frozen at an average set voltages to correct for common static aberrations in the telescope and instrument. More details of the observations and image data reduction are presented in.¹¹

For nearly all nights, simultaneous data were obtained from the MASS/DIMM seeing monitor on Maunakea (MKAM) at the nearby Canada France Hawaii Telescope *. These data report the turbulence strength and corresponding seeing from high altitude layers at 500 m and above from the MASS and integrated over the whole atmosphere from the DIMM. The cumulative distribution of total and free-atmosphere seeing during the RUN3-RUN5 nights are shown in Figure 1. For these nights the average seeing was 0.65" and the median free-atmosphere seeing was 0.37". We note that the distribution of free-atmosphere seeing is not log-normal as expected and as seen in the distribution of long-term free-atmosphere seeing measured by MKAM but rather bimodal - with some nights with exceptionally weak free-atmosphere seeing.

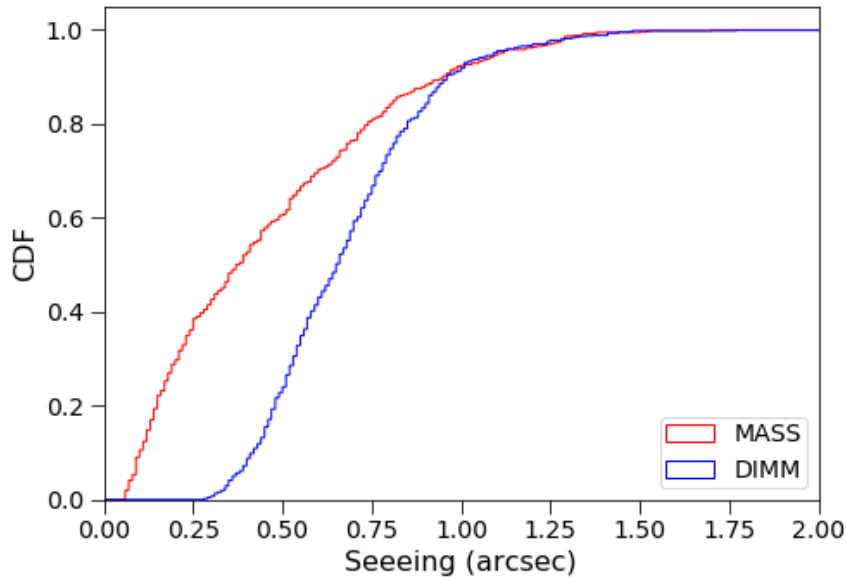


Figure 1. MASS/DIMM measurements of the total (DIMM) and free-atmosphere seeing (MASS) during the imaka GLAO runs to date. The median DIMM seeing is comparable to the long term median since the MASS/DIMM was installed on the summit ridge (2009). Note that the histogram of the MASS seeing does not show the expected log-normal distribution so it is likely that the conditions during the imaka runs is not representative of the long term conditions.

3.2 Science Image Quality

All image data were fit with Moffat profiles.¹² The 1-dimensional Moffat formalization $I(r) = I_0[1 + (r/\alpha)^2]^{-\beta}$ illustrates the role of the two Moffat parameters. The width of the image is represented in α while the shape of the PSF is represented in the β . The FWHM depends on both. For the imaka image data we fit a 2-dimensional Moffat profile¹¹ in order to account for any non-axial symmetric terms. In the case of the GLAO-off images, there is a clear elongation that appears to be associated with the right-ascension tracking of the telescope. For this paper we note the "GLAO-off" image quality as the FWHM of the minor axis of the Moffat fit but we note that wind-shake and tracking errors are common to most ground based telescopes. The GLAO corrected PSFs are round to better than the our measured variation of the plate scale across the field.

GLAO improves the delivered image quality for guide stars are separated by 15-17". Figure 3.2 shows the distribution of GLAO-off and GLAO-on image FWHM. The improvement in FWHM based on nightly averages is between 1.3 and 2.8x¹¹ and amounts to a shift of the FWHM distribution toward better image quality by

*<http://mkwc.ifa.hawaii.edu/current/seeing/>

about 0.25-0.3". This improvement appears to be constant over most seeing conditions. However, the steepening of the GLAO PSF FWHM CDF at good FWHM values suggests an instrumental error that limits the image quality under good seeing conditions.

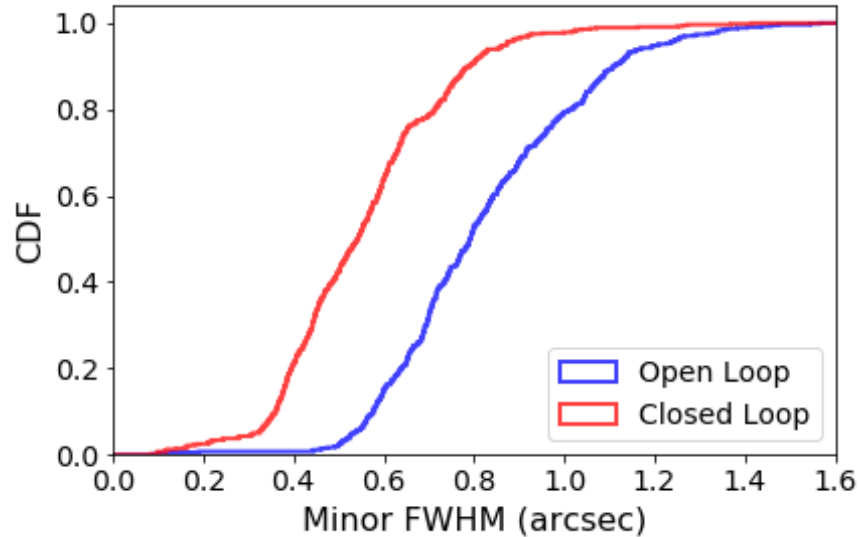


Figure 2. The distribution of measured FWHM for the GLAO-on (“closed-loop”) and GLAO-off (“open loop”) images during RUN3-RUN5 at the University of Hawaii 2.2-meter telescope. The FWHM are derived from the minor axis of the 2-dimensional Moffat profile fits. All quantities are given at a wavelength of 0.5um and no zenith angle correction has been applied. The median GLAO-on and GLAO-off FWHM are 0.8” and 0.5” respectively.

The GLAO PSFs are sharpened but we find that the shape is PSF also changes as a result of the GLAO correction. The wings of the GLAO corrected PSF are shallower than the uncorrected PSFs (i.e. more flux in the wings). This effect is seen in our simulations and we speculate that it is due to the residual ground-layer phase aberrations. In particular, the limited number of actuators on the ‘imaka DM gives a partial ground-layer correction in the visible that leaves a relatively large halo in the PSF. We expect that at longer wavelengths this effect will be reduced.

3.3 Discussion on Image Quality

A direct comparison between the seeing monitor’s integrated and free-atmosphere seeing in general does not agree well with the delivered image quality (DIQ) - GLAO correction or not (Figure 3.3. The seeing monitor’s DIMM measures the integrated seeing seven meters off the surface approximately 100 meters North of the UH 2.2meter telescope while the GLAO-off image FWHM is a delivered image quality at the focal plane of the telescope that includes aberrations that are not seen by the seeing monitor such as dome/tube seeing, telescope jitter (wind shake and tracking errors), and any residual static aberrations in the telescope and instrument. Similarly the seeing monitor’s MASS provides an integral of the estimated turbulence from an altitude of approximately 500 meters and higher while the GLAO FWHM are again a delivered image quality at the telescope focal plane that contains aberrations not common to the MASS measurements. Examples of nightly variations of these four measurements from the May 2017 observations are shown in Figure 3.3. On the night of 17 May 2017, the temperature in the dome was considerably warmer than the outside air and the GLAO-off DIQ is considerably worse than the integrated seeing measured by the seeing monitor. On other nights the seeing and GLAO-off FWHM are closer but in general the uncorrected DIQ is worse than the seeing measured by the seeing monitor. The more interesting comparison is with the GLAO image FWHM and the estimated free-atmosphere seeing. Here again the GLAO focal plane images are in general worse than the free-atmosphere seeing measured by the MASS. There, in fact, appears to be a floor of about 0.3” for the ‘imaka images.

As noted in the discussion on the error budget, the residual free atmosphere is just one contribution to the delivered image quality so in comparing any estimate of the free-atmosphere seeing to the GLAO image FWHM

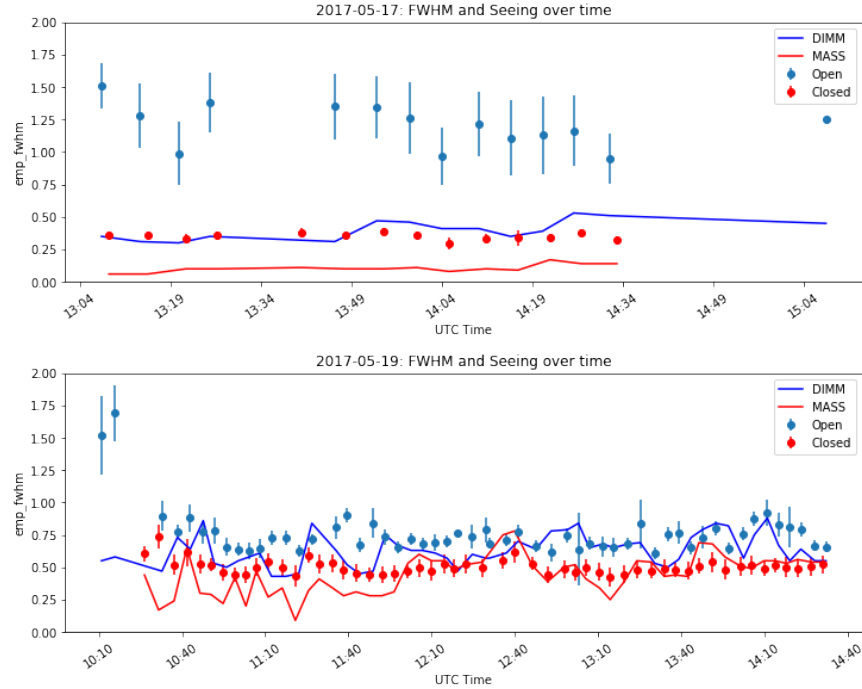


Figure 3. Example of time dependence of GLAO-off and GLAO-on images on two nights. The dome seeing on the night of 17 May 2017 was particularly bad.

we need to account for the additional image quality error terms. After the residual free atmosphere the two next largest terms are the the free-atmosphere tomographic error and the "implementation" errors. The optical design and the AO implementation errors amount to an aberration of $FWHM_{inst} \sim 0.13''$ independent of the seeing. The tomographic error injects some of the free-atmosphere variance into the GLAO correction and effectively worsens the free-atmosphere seeing by a factor of $(1 + 1/N_{WFS})^{3/5}$. For $N_{WFS} = 4$ this factor is 1.14. Over all nights, these additional error terms amount to a FWHM that is 0.08-0.14" larger than the free-atmosphere seeing. Figure 3.3 shows the cumulative distribution of the GLAO image FWHM, the MASS seeing, and an estimate of the free-atmosphere seeing derived from the GLAO-off AO telemetry taken closely in time to the GLAO images. The roughly 0.1" correction of the telemetry derived free-atmosphere seeing CDF to larger values brings the the CDF in good agreement with the GLAO FWHM distribution. However, the MASS seeing distribution, except possible for its median value, does not agree with the telemetry or the GLAO FWHM.

4. CONCLUSIONS

We find that GLAO on Maunakea provides improvements to the delivered image quality on the UH 2.2-meter telescope even when the guide stars are separated by distances of 15-16 arcminutes. The FWHM are improved by a factor of 1.3-2.7x in the visible depending on the seeing conditions. The GLAO image quality, when corrected for the additional error terms in the instrument matches that predicted by the free-atmosphere seeing measured in the AO telemetry stream but do not match that predicted by the MASS unit on the Mauna Kea Seeing monitor.

Future work will explore the dependence of the GLAO correction on different guide star asterisms, imaging wavelength, and control algorithm.

ACKNOWLEDGMENTS

The current 'imaka work is funded by the National Science Foundation (AST-1310706) and the Mt. Cuba Foundation.

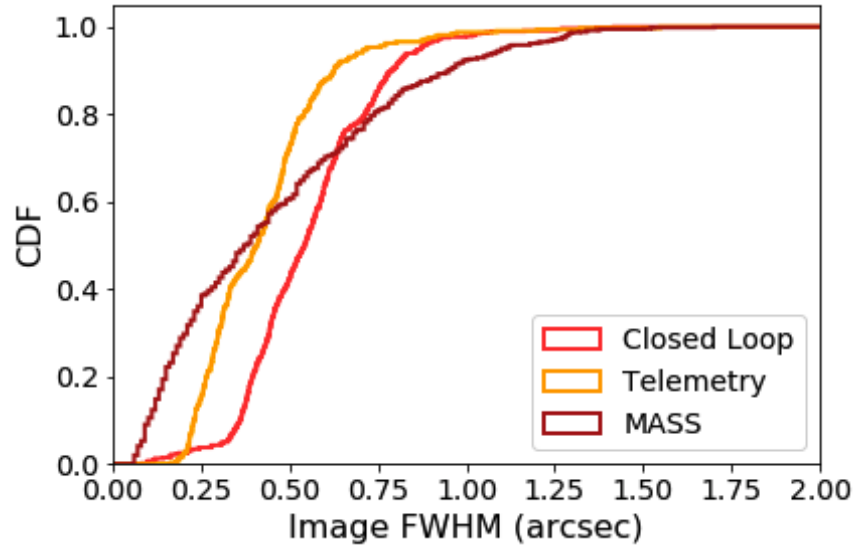


Figure 4. Comparison of the distribution of GLAO image FWHM, the seeing monitor MASS measurements, and the free-atmosphere seeing estimated from the GLAO-off AO telemetry. The offset between the CDFs of the telemetry derived free-atmosphere seeing and the GLAO FWHM is about 0.14". Its slightly less at good seeing values and slightly worse under poor seeing conditions.

REFERENCES

- [1] Tokovinin, A., Cantarutti, R., Tighe, R., Schurter, P., Martinez, M., Thomas, S., and van der Blik, N., "SOAR Adaptive Module (SAM): Seeing Improvement with a UV Laser," *PASP* **128**, 125003 (Dec. 2016).
- [2] Orban de Xivry, G., Rabien, S., Busoni, L., Gaessler, W., Bonaglia, M., Borelli, J., Deysenroth, M., Esposito, S., Gemperlein, H., Kulas, M., Lefebvre, M., Mazzoni, T., Peter, D., Puglisi, A., Raab, W., Rahmer, G., Sivitilli, A., Storm, J., and Ziegler, J., "First on-sky results with ARGOS at LBT," in [*Adaptive Optics Systems V*], *Proc. SPIE* **9909**, 990936 (July 2016).
- [3] La Penna, P., Aller Carpentier, E., Argomedo, J., Arsenault, R., Conzelmann, R. D., Delabre, B., Donaldson, R., Gago, F., Gutierrez-Cheetam, P., Hubin, N., Jolley, P., Kiekebusch, M., Kirchbauer, J. P., Klein, B., Kolb, J., Kuntschner, H., Le Louarn, M., Lizon, J.-L., Madec, P.-Y., Manescau, A., Mehrgan, L., Oberti, S., Quentin, J., Sedghi, B., Ströbele, S., Suárez Valles, M., Soenke, C., Tordo, S., and Vernet, J., "AOF: standalone test results of GALACSI," in [*Adaptive Optics Systems V*], *Proc. SPIE* **9909**, 99092Z (July 2016).
- [4] Chun, M. R., Lai, O., Toomey, D., Lu, J. R., Baranec, C., Thibault, S., Brousseau, D., Zhang, H., Hayano, Y., and Oya, S., "imaka: a path-finder ground-layer adaptive optics system for the University of Hawaii 2.2-meter telescope on Maunakea," in [*Adaptive Optics Systems IV*], *Proc. SPIE* **9148**, 91481K (Aug. 2014).
- [5] Chun, M. R., Lai, O., Toomey, D., Lu, J. R., Service, M., Baranec, C., Thibault, S., Brousseau, D., Hayano, Y., Oya, S., Santi, S., Kingery, C., Loss, K., Gardiner, J., and Steele, B., "Imaka: a ground-layer adaptive optics system on Maunakea," in [*Adaptive Optics Systems V*], *Proc. SPIE* **9909**, 990902 (July 2016).
- [6] Lai, O., Chun, M. R., Pazder, J., Véran, J.-P., Jolissaint, L., Andersen, D., Salmon, D., and Cuillandre, J.-C., "Imaka: a Lagrange invariant of ELTs," in [*Adaptive Optics Systems II*], *Proc. SPIE* **7736**, 77361D (July 2010).
- [7] van Dam, M. A., Bouchez, A. H., and McLeod, B. A., "Wide field adaptive optics correction for the GMT using natural guide stars," in [*Adaptive Optics Systems IV*], *Proc. SPIE* **9148**, 914813 (July 2014).
- [8] Chun, M. R., Lai, O., Butterley, T., Goebel, S., Baranec, C., and Toomey, D., "Extremely high-resolution ground-layer optical turbulence profile at Mauna Kea," in [*Adaptive Optics Systems IV*], *Proc. SPIE* **9148**, 914867 (Aug. 2014).

- [9] Schöck, M., Els, S., Riddle, R., Skidmore, W., Travouillon, T., Blum, R., Bustos, E., Chanan, G., Djorgovski, S. G., Gillett, P., Gregory, B., Nelson, J., Otárola, A., Seguel, J., Vasquez, J., Walker, A., Walker, D., and Wang, L., “Thirty Meter Telescope Site Testing I: Overview,” *PASP* **121**, 384 (Apr. 2009).
- [10] Chun, M., Wilson, R., Avila, R., Butterley, T., Aviles, J.-L., Wier, D., and Benigni, S., “Mauna Kea ground-layer characterization campaign,” *MNRAS* **394**, 1121–1130 (Apr. 2009).
- [11] Abdurrahman, F., Lu, J. R., Chun, M., Service, M. W., Lai, O., Fohring, D., Toomey, D., and Baranec, C., “Improvements in Image Quality with the ‘imaka Ground Layer Adaptive Optics System,” *in preparation* (2017).
- [12] Moffat, A. F. J., “A Theoretical Investigation of Focal Stellar Images in the Photographic Emulsion and Application to Photographic Photometry,” *AAP* **3**, 455 (Dec. 1969).